S100A6 Amyloid Fibril Formation Is Calcium-modulated and Enhances Superoxide Dismutase-1 (SOD1) Aggregation

Hugo M. Botelho, Sónia S. Leal, Isabel Cardoso, Kiran Yanamandra, Ludmilla A. Morozova-Roche, Günter Fritz and Cláudio M. Gomes

Abstract

S100A6 is a small EF-hand calcium- and zinc-binding protein involved in the regulation of cell proliferation and cytoskeletal dynamics. It is overexpressed in neurodegenerative disorders and a proposed marker for Amyotrophic Lateral Sclerosis (ALS). Following recent reports of amyloid formation by S100 proteins, we investigated the aggregation properties of S100A6. Computational analysis using aggregation predictors Waltz and Zyggregator revealed increased propensity within S100A6 helices H_I and H_{IV}. Subsequent analysis of Thioflavin-T binding kinetics under acidic conditions elicited a very fast process with no lag phase and extensive formation of aggregates and stacked fibrils as observed by electron microscopy. Ca^{2+} exerted an inhibitory effect on the aggregation kinetics, which could be reverted upon chelation. An FT-IR investigation of the early conformational changes occurring under these conditions showed that Ca^{2+} promotes anti-parallel β-sheet conformations that repress fibrillation. At pH 7, Ca^{2+} rendered the fibril formation kinetics slower: time-resolved imaging showed that fibril formation is highly suppressed, with aggregates forming instead. In the absence of metals an extensive network of fibrils is formed. S100A6 oligomers, but not fibrils, were found to be cytotoxic, decreasing cell viability by up to 40%. This effect was not observed when the aggregates were formed in the presence of Ca^{2+}. Interestingly, native S1006 seeds SOD1 aggregation, shortening its nucleation process. This suggests a cross-talk between these two proteins involved in ALS. Overall, these results put forward novel roles for S100 proteins, whose metal-modulated aggregation propensity may be a key aspect in their physiology and function.

Keywords

Aggregation; Amyloid; Biophysics; Protein Aggregation; S100 Proteins; Superoxide Dismutase (SOD)

Introduction

S100 proteins comprise a family of EF-hand calcium-binding proteins. They represent central regulators involved in cell cycle control, cell growth, differentiation, and motility in vertebrates. In humans, 21 different S100 paralogs are expressed (1). These proteins have organ- and tissue-specific expression patterns, and their biological activity is modulated by different metal ions, namely calcium (Ca^{2+}), zinc (Zn^{2+}), and copper (Cu^{2+}). Metal ion binding to S100 proteins regulates conformation and, in some instances, oligomerization of S100 dimers into higher order oligomers (2, 3). A common feature in S100 proteins is Ca^{2+} binding via EF-hand motifs which triggers the exposure of an inter-helical hydrophobic protein interaction site (1). This allows binding and regulation of different signaling molecules translating the Ca^{2+} signal into a cellular response (4, 5). Some family members also bind Zn^{2+} and Cu^{2+} at secondary binding sites with high affinity, and the binding of these metals is usually associated to subtle conformational changes (2).

The remarkable conformational plasticity of S100 proteins and the regulatory capacity of metal ions was recently further extended by the report that the proinflammatory S100A8/A9 heterodimer forms amyloid deposits. These were found in prostatic inclusions called *corpora amylacea* from cancer patients, and protein deposition *in vitro* was facilitated by Ca^{2+} and Zn^{2+} (6). Clearly, protein deposition phenomena are becoming increasingly relevant also in cancer (7,–, 9). This finding opened the question whether other S100 proteins are capable to form amyloids too and whether such amyloids are involved in other diseases

as well. Most interestingly, several S100 proteins have been reported to occur at largely elevated levels in neurodegenerative disorders (10,–,13).

Underlining the importance of S100 signaling, a number of S100 proteins show altered expression levels in cancer and neurodegenerative, inflammatory, and auto-immune diseases (14). A paradigmatic example is S100A6, which regulates cell proliferation, cytoskeletal dynamics and tumorigenesis (15) in response to Ca^{2+} binding. This protein is overexpressed in Alzheimer disease (AD)[2] (10, 11) and Amyotrophic Lateral Sclerosis (ALS), a disease characterized by progressive degeneration of motor neurons. In ALS patients, S100A6 is largely overexpressed in reactive astrocytes located in the brainstem and spinal cord, surrounding impaired motor neuron axons (11). In turn, these ALS-affected neurons contain cytoplasmic aggregates of Cu/Zn Superoxide Dismutase (SOD1), which are ubiquitous disease indicators (16). For this reason, S100A6 has been proposed as a marker for ALS (17). Also, in AD, S100A6 is up-regulated in the brain white matter as well as in gray matter astrocytes surrounding the Aβ senile plaques, both in human patients and mouse models (10).

Following these relationships, we here report the identification and characterization of S100A6 as an amyloidogenic protein, and we undertake a detailed characterization of the role of Ca^{2+} as a modulator of fibril assembly, morphology and structural properties. The biophysical findings are framed in respect to the possible biological implications of this finding, through the analysis of the effect of metal ions on the cytotoxicity of amyloids and in respect to amyloid cross seeding with SOD1.

MATERIALS AND METHODS

Chemicals and Proteins

All reagents were of the highest grade commercially available. Thioflavin T was obtained from Sigma. Hen egg white lysozyme was obtained from Fluka. A Chelex resin (Bio-Rad) was used to remove contaminant trace metals from all solutions. S100A6 was expressed and purified to homogeneity using reported protocols (18). SOD1 expression, and purification were performed as in Ref. 19 and preparation of the apo-form as in Ref. 20. Protein quantification was made using Bradford's method (21).

Amyloidogenic Propensity Analysis

The amyloidogenic propensity of S100A6 at pH 7 was computed using the Waltz (22) and Zyggregator (23, 24) web servers.

S100A6 Aggregation Assays

Amyloidogenesis and fibril formation assays were performed as described previously (25). Briefly, S100A6 was diluted into either 50 mM glycine, pH 2.5, or 50 mM Tris, pH 7. Centrifugation at 12,000 × *g* for 10 min at 4 °C removed any insoluble material before aggregation assays. Final S100A6 concentration was 3 mg/ml (295 μM). When required, a 10-fold molar excess of $CaCl_2$ or $ZnCl_2$ (2.9 mM) was added. Amyloid formation was promoted by quiescent incubation at 57 °C (pH 2.5) or at 37 °C under 1000 rpm orbital agitation (pH 7). Lysozyme amyloids were generated by incubating 10 mg/ml protein in 50 mM glycine pH 2.5 at 57 °C, as described previously (26).

Thioflavin-T Fluorescence

The ThT fluorescence assay for the detection of amyloid was performed as described previously (26). At different time points, 15 μg of S100A6 or 50 μg of lysozyme were diluted in buffer and incubated under stirring for 2 min at 25 °C. Fluorescence (482 nm) was recorded with a Cary Varian Eclipse instrument upon excitation at 440 nm using a PMT voltage of 600 V and excitation and emission slits of 10 nm.

Circular Dichroism (CD) Spectroscopy

CD experiments were performed using a Jasco J-815 spectropolarimeter equipped with a Peltier-controlled thermostated cell support. Far UV CD spectra and 1 °C/min thermal denaturation curves (as

reported by the CD at 222 nm) were recorded for 0.1 mg/ml S100A6 (9.8 µM) in either 50 mM KP_i pH 7 or 50 mM glycine, pH 2.5. Spectra were deconvoluted with CDNN 2.1.

Dynamic Light Scattering

The mean light scattering intensity variations were determined with a Malvern Instruments Zetasizer Nano ZS instrument. Backscattered 633 nm laser light from fifteen 10 s accumulations was averaged to retrieve light scattering intensity and average particle size from the intensity distribution using the Malvern Instruments DTS software and a multimodal fit with quadratic weighting and 0.01 regulariser.

Transmission Electron Microscopy

For visualization by TEM, 5-µl sample aliquots were absorbed to carbon-coated collodion film supported on 400-mesh copper grids, and negatively stained with 1% uranyl acetate. The grids were exhaustively visualized with a Jeol microscope (JEM-1400), operated at 80 kV.

ATR FT-IR Spectroscopy

The secondary structure of apo and Ca^{2+}-S100A6 was monitored during amyloid formation assays at pH 2.5 by ATR FT-IR measurements performed in a Bruker IFS 66/S spectrometer equipped with a MCT detector and a thermostatized Harrick BioATR II cell. The spectrometer was set to 1 min accumulation time, 12 mm aperture, 20 kHz scanner velocity, and 4 cm^{-1} spectral resolution. Band assignments were based on typical absorption regions for specific secondary structure elements (27).

Cytotoxicity

The cytotoxicity of S100A6 toward human neuroblastoma SH-SY5Y cells was assessed by the reduction of the chromogenic electron acceptor WST-1 (Roche) (28). Cells were cultured in DMEM supplemented with 10% (v/v) FBS and antibiotics in a 5% CO_2 humidified atmosphere at 37 °C. After seeding in 96-well plates (10^4 cells/well), cells were grown overnight and incubated with 5 µM S100A6 in 100 µl FBS-free medium during 48 h. Then, 10 µl of WST-1 was added and 4 h later absorbance at 450 nm was read with a Labsystem Multiscan RC. Cell viability was normalized to the reading obtained with cells incubated without S100A6. Statistical differences were assessed with double-tailed, two sample unequal variance Student's *t* test.

Dot-blot Analysis

The reactivity of S100A6 oligomers against conformation-dependent antibodies was carried out in a dot-blot analysis as described in Ref. 29 using the anti-amyloid fibrils OC antibody (AB2286 Merck Millipore) and the A11 anti amyloid oligomer antibody (AB9234 Merck Millipore).

SOD1-S100A6 Cross-seeding

For assessing the effect of S100A6 in SOD amyloidogenesis, 50 µM apo SOD1 was incubated in 50 mM Tris, pH 7.3, 5 mM TCEP, and 100 µM ThT at 37 °C with and without 2% native apo S100A6 (1 µM) in black 96-well plates (Nunc FluoroNunc). One (1/8 in) teflon bead was added, and the plate was agitated at 600 rpm during incubation. Real time ThT fluorescence (480 nm) was recorded using a BMG Fluostar Optima fluorescence plate reader upon excitation at 440 nm. Curve analysis and lag time determination was carried out as described in Ref. 30.

RESULTS

S100A6 Hydrophobic Core Has Amyloidogenic Propensity

The S100A6 primary sequence was analyzed for amyloid-prone segments using two complementary computational algorithms: Waltz (22) and Zyggregator (23, 24). Both algorithms provide position-specific scores, which can be used to identify amyloidogenic hot spots in the sequence. Whereas Waltz relies on a combination of amyloid-prone sequence pattern recognition based on physicochemical properties and homology modeling, Zyggregator correlates sequence information with experimental aggregation rate

changes upon mutation and polypeptide physicochemical properties. Both algorithms predict significant aggregation prone regions in helices H_I (residues 11–18) and H_{IV} (residues 71–82), within the hydrophobic core of S100A6 (Fig. 1). The regions with significant scores identified by Waltz (Fig. 1, *gray bars*) indeed correspond to regions with high Zyggregator scores (Z_{agg}). Noteworthy, Z_{agg} scores for S100A6 have a magnitude similar to those for $A\beta_{1-42}$, the major aggregating peptide involved in AD (23). Altogether, these results suggest that S100A6 comprises aggregation prone segments, which may trigger amyloid fibril formation.

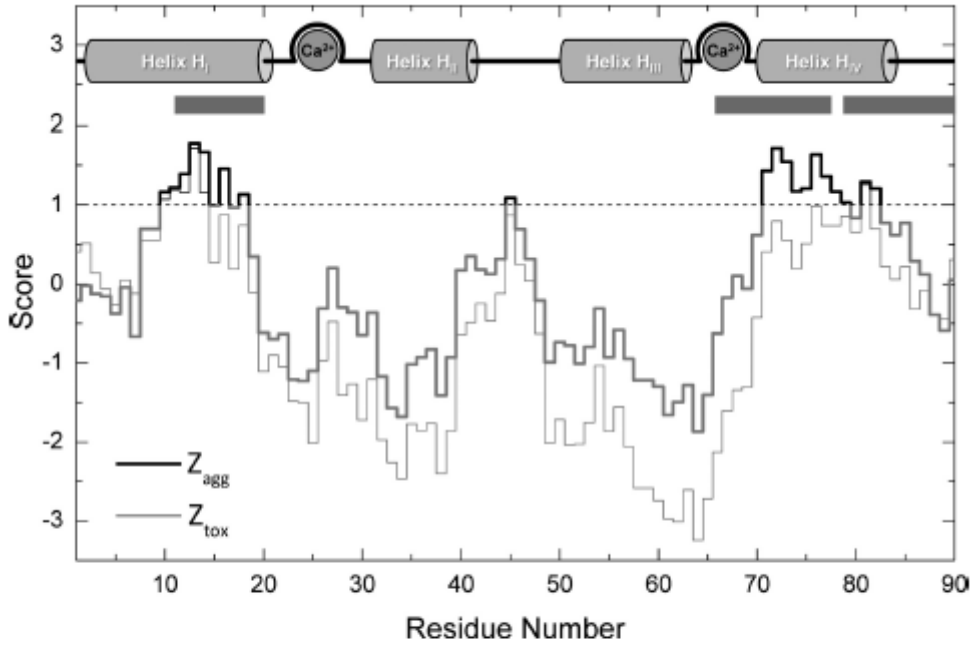

FIGURE 1. **Amyloidogenic propensity analysis of S100A6.** The sequence-dependent amyloidogenic propensity at neutral pH was computed by the Zyggregator and Waltz algorithms. Zyggregator was used to retrieve intrinsic fibril formation propensity (Z_{agg}) and protofibril/oligomer formation propensity scores (Z_{tox}). Significant scores for amyloidogenesis are above 1. Waltz reports on fibrillization propensity. Horizontal gray bars represent significant Waltz scores (~98%). The top scheme represents S100A6 topology.

S100A6 Forms Amyloid-like Fibrils

We then carried out an exploratory analysis of amyloid formation by S100A6 using conditions known to induce fibril formation in the well-established model lysozyme, which was used as a positive control. Therefore, under acidic conditions and high temperature (pH 2.5 and 57 °C), we observed a very fast buildup of S100A6 ThT-reactive species, which developed into fibrils after 10 days of incubation (Fig. 2). The formation of lysozyme fibrils under these experimental conditions served as a reference to assess S100A6 amyloid formation in a reasonable time frame. Interestingly, the sigmoidal shape of the aggregation kinetic profile typical for lysozyme was not observed for S100A6 which was rather concave-like (30) (Fig. 2*A*). The absence of a lag phase reflects an instantaneous nucleation process and suggests a high propensity of S100A6 to form directly growth-nuclei from its soluble conformation. Structural analysis by far-UV CD showed that S100A6 is not unfolded neither at acidic pH (of 2.5) nor at higher temperature (of 57 °C), thus clearly ruling out that aggregate formation is triggered from unfolded protein. Nevertheless, acidic conditions resulted in a conformation which retains its compactness, but has an altered network of interactions which results in a decreased α-helical content with a corresponding increase in β-sheet structures (~4%). In fact, ultrastructural analysis by transmission electron microscopy (TEM) corroborated the presence of S100A6 fibrillar oligomers and protofilaments (Fig. 2, *B* and *C*). The

fibrillar structures formed at pH 2.5 after 28 days were polymorphic and fibrils with different widths were observed: 4–5 nm wide fibrils (*black arrow*, Fig. 2*B*), 15 nm wide fibrils (*black arrowhead*, Fig. 2*B*), and several other thicker fibrils. Thick fibrils consisting of several smaller fibrils with 4–5 nm width were observed (*white arrows*, Fig. 2*B*). The long 4–5 nm wide protofibrils might undergo lateral association and represent building blocks of the larger fibrils. Nevertheless, considering the observed kinetic profile, such a mechanism would have a minor contribution to the overall process. In other cases, it is suggested that mature fibrils are instead produced by longitudinal growth of full-width species (31, 32). Indeed, this pathway might also apply for the formation of S100A6 fibrils since thick but short structures are observed (see *e.g. white arrow*, Fig. 2*B*). Furthermore, a detailed analysis of the TEM image revealed the assembly of structures with ~15 nm of width, into an already partially formed fibril (Fig. 2*C*). Thus, it is possible that under the chosen conditions both mechanisms play a critical role during S100A6 fibril formation.

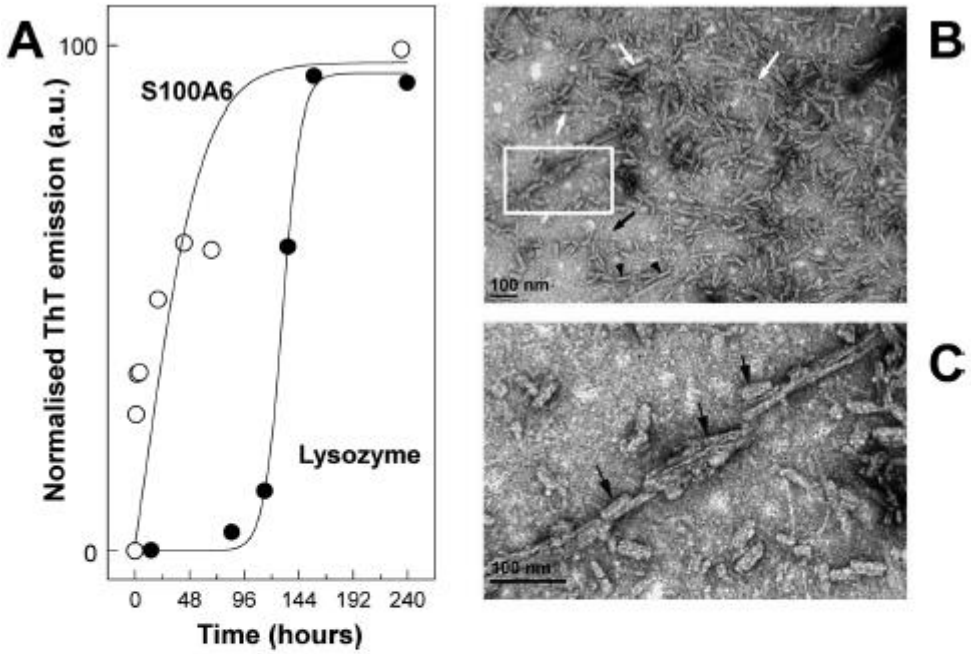

FIGURE 2. **S100A6 forms amyloid fibrils.** *A*, formation of S100A6 amyloid at pH 2.5 and 57 °C (3 mg/ml) was monitored by the ThT fluorescence assay. Lysozyme (10 mg/ml) is a positive control, owing to the well characterized amyloidogenesis at the same conditions. The plot represents the normalized variation of the ThT emission in respect to the end point. The solid lines guide the eye as a clear plateau is not defined. *B*, after 28 days of incubation at 37 °C, TEM analysis revealed a polymorphic fibril structure encompassing 4–5 nm wide fibrils (*black arrows*), 15 nm wide fibrils (*black arrowhead*), short thick fibrils composed by the association of several 4–5 nm wide fibrils (*white arrows*) and several other thicker fibrils. *C*, magnification of *panel B* (*white rectangle*), highlighting the association of 15 nm of wide structures (*black arrows*) into a larger fibril.

Ca^{2+} Modulates Aggregation and Induces Structural Changes at Early Phases of Fibril Formation

Because S100A6 is a Ca^{2+}- and Zn^{2+}-binding protein, we have subsequently investigated the conformational changes occurring at the earliest stages of S100A6 aggregation, and the effect of these metal ions on this process. We started by using dynamic light scattering to investigate the aggregation of S100A6, in the presence and absence of Ca^{2+} (Fig. 3*A*) No lag phase was observed and light scattering aggregates were formed up to reaching a plateau, irrespective of the presence of Ca^{2+}. We then moved to investigate the ThT binding properties of these S100A6 aggregates (Fig. 3*B*). The results showed that aggregates formed starting from apo S100A6 are ThT reactive from the early stages of the aggregation

process. However, the presence of metal ions resulted in aggregates with different ThT-binding behaviors: whereas Zn^{2+} had a negligible effect, Ca^{2+} repressed ThT-binding (Fig. 3*B*). The combination of light scattering and ThT-binding data suggests that Ca^{2+} induces the formation of aggregates that are not amyloidogenic and do not bind ThT. However, the possibility that Ca^{2+} exerts an inhibitory effect on the fibrillation process cannot be ruled out at this stage. Whatever the scenario, the fact is that Ca^{2+} modulates S100A6 aggregation. Accordingly, addition of EDTA to chelate Ca^{2+} and revert S100A6 into its apo form promptly restored the formation of ThT-positive species (Fig. 3*B*, *arrow*). An investigation of the reactivity of these oligomeric species against conformational antibodies indicated no interaction toward the anti-amyloid fibrils antibody and very weak reactivity toward the amyloid oligomer. The structural differences between the apo and Ca^{2+}-bound S100A6 conformers produced under these acidic conditions and high temperature were investigated using Fourier transform infrared (FT-IR) spectroscopy. The amide I region of the infrared spectrum (1600–1700 cm^{-1}) provides quantitative information on secondary structure, being especially sensitive to β-sheet conformations (Fig. 3*C*). A direct comparison of the amide I band in the presence and in the absence of Ca^{2+} at identical incubation times (~2 h) revealed significant structural differences. During the incubation in the presence of Ca^{2+} two spectral features developed: a local maximum at 1625 cm^{-1} and a shoulder at 1690 cm^{-1}, which are very prominent in the difference spectrum (Fig. 3*D*). This combination of bands is characteristic of an anti-parallel β-sheet conformation, indicative of oligomeric species structurally distinct from fibrils (33). This observation is in agreement with the residual ThT binding observed in the presence of Ca^{2+} (Fig. 3*B*). A negative band at 1650 cm^{-1} is also observed in the difference spectrum, indicative of a decrease in α-helix content in the Ca^{2+}-bound form. Altogether, these results show that binding of Ca^{2+} to S100A6 results in the formation of aggregated species which are off-pathway in respect to amyloid fibril formation.

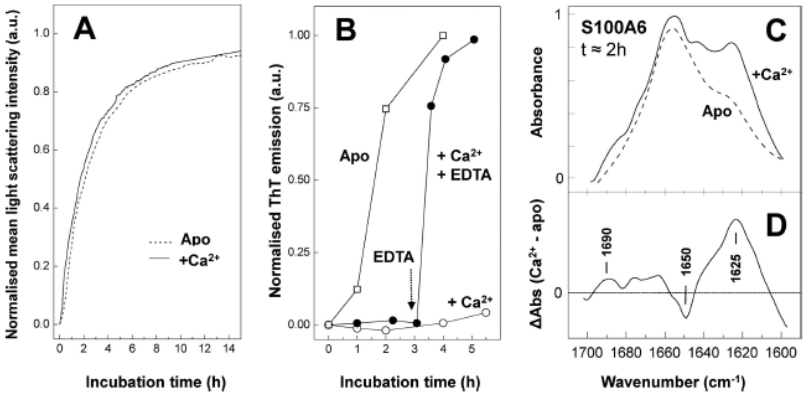

FIGURE 3. **Calcium modulates structural changes at early phases of fibril formation** The kinetics of amyloid formation by S100A6 (3 mg/ml) at pH 2. 5 and 57 °C was determined by DLS (*A*) and the ThT fluorescence assay (*B*). In both cases, amyloidogenesis occurred without a lag phase. Light scattering aggregates were formed irrespective of the presence of Ca^{2+} (*A*). In the ThT assay (*B*), aggregation kinetics was equivalent for S100A6 in the apo form (□) or in the presence of Zn^{2+} (2.9 mM). Ca^{2+} (2.9 mM, ○) completely inhibited amyloidogenesis in this time scale. However, Ca^{2+} chelation by excess EDTA (●, EDTA addition indicated by *arrow*) restored apo-like amyloidogenesis. The plot represents the normalized variation of the ThT emission in respect to end points. The *solid lines* are used to guide the eye. *C*, amide I FT-IR absorption spectra of apo (- - -) and Ca^{2+}-S100A6 (——) after 2 h incubation at pH 2.5 and 57 °C. *D*, difference spectrum derived from *C* (Ca^{2+}-apo). Incubation in the presence of Ca^{2+} leads to the accumulation of anti-parallel β-sheets (contributions at 1625 cm^{-1} and 1690 cm^{-1}) and the loss of α-helices (1650 cm^{-1}), indicating structurally distinct conformations in the two preparations.

S100A6 Fibrillates under Physiological Conditions

The formation of S100A6 amyloid-like fibrils was further investigated at physiological conditions (pH 7 and 37 °C). As anticipated, the process of S100A6 aggregation at neutral pH was much slower, and proceeded via a sharper sigmoid-type transition (Fig. 4*A*). The absence of an evident lag phase suggests that the formation of the aggregation-nuclei readily takes place from the soluble conformers. In contrast, the Ca^{2+}-bound S100A6 conformers are less prone to generate aggregation-nuclei, as evidenced by a lag phase like period (Fig. 4*A*). The more extensive growth phase and higher intensity of ThT binding by apo S100A6 also suggests higher levels of fibrillization. In fact, this was corroborated by TEM analysis which showed a higher fibril content in the apo form, whereas the presence of Ca^{2+} mainly yielded amorphous aggregates (Fig. 4, *B*–*E*). Analysis of the aggregated species obtained after 28 days of incubation showed mostly large amorphous aggregates have formed (Fig. 4*B*), independently of the presence of Ca^{2+} (Fig. 4*D*). Extending the incubation for 65 days resulted in increased fibrillogenesis: long fibrils were detected (Fig. 4*C*), although aggregates were still the most abundant species. Such fibrils were negligible in the presence of Ca^{2+} (Fig. 4*E*), revealing that Ca^{2+} refrains fibril formation and leads essentially to the formation of small aggregates. These results indicate that also under physiological conditions Ca^{2+} perturbs the formation of

S100A6 amyloid fibrils by favoring off pathway oligomers at the expenses of fibrillization competent species. The morphological properties of apo S100A6 fibrils produced over longer time scales were analyzed in more detail by TEM (Fig. 5). Continued incubation at 37 °C for 84 days resulted in abundant fibril formation. In contrast to the acidified preparations, we did not observe various fibril types: the preparation became very homogenous and prominent 7–8 nm wide fibrils were present (Fig. 5*A*). After extended incubation for 116 days, the fibrils started to form bundles (Fig. 5*B*) accompanied by additional intertwining and tangling.

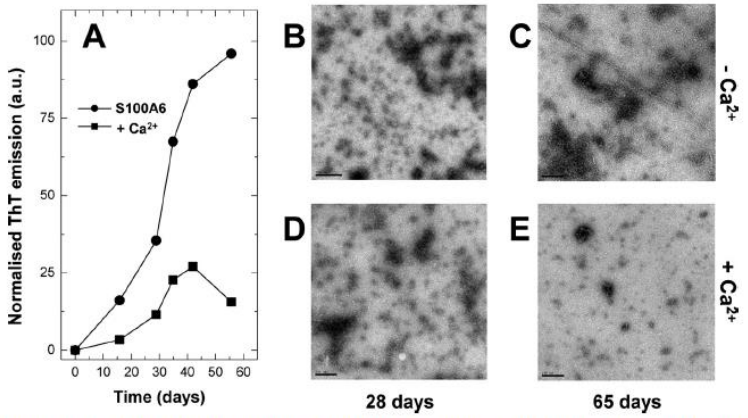

FIGURE 4. **Amyloid fibril formation by S100A6 under physiological conditions.** *A*, amyloid formation kinetics for apo (●) and Ca^{2+}-S100A6 (■) at pH 7, 37 °C, 3 mg/ml and 1000 rpm, as derived from the ThT fluorescence assay. Under these conditions, Ca^{2+} partially inhibits amyloid formation. TEM analysis of apo S100A6 at 28 (*B*) and 65 days incubation (*C*). TEM analysis of Ca^{2+}-S100A6 at 28 (*D*) and 65 days incubation (*E*). At lower incubation times large amorphous aggregates are the prevalent structures, which partially assemble into long fibrils in apo but not Ca^{2+}-S100A6. Scale bars: 200 nm.

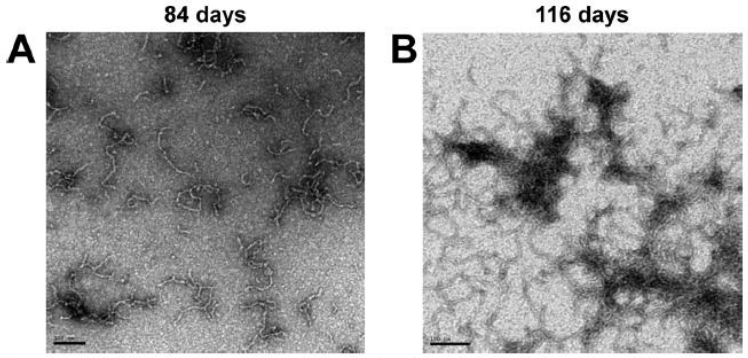

FIGURE 5. **Morphology of S100A6 amyloid fibrils.** Upon prolonged incubation of S100A6 (3 mg/ml) at pH 7, 37 °C and 1000 rpm, the amyloid population became homogenous. *A*, after incubating S100A6 for 84 days 7–8 nm wide fibrils were observed, which formed bundles when further incubated until 116 days (*B*). Scale bars: 100 nm.

Toxicity of S100A6 Oligomers and Fibrils

S100A6 is a predominantly intracellular protein but also exerts an extracellular action via binding and subsequent activation of the receptors for advanced glycation endproducts (RAGE), a pattern recognition receptor (15, 34). Considering the new amyloidogenic properties of S100A6 and the fact that insoluble protein aggregates are frequently associated with toxic gains of function and cellular toxicity, we have thus investigated the toxicity of S100A6 oligomers and fibrils. For this purpose we used the human neuroblastoma SHSY-5Y cell line as a model system: upon challenging these cells with different S100A6 conformers (native protein, oligomers, and amyloid fibrils), cell viability was determined by the WST-1 reduction assay. Also, considering the inhibitory effect of Ca^{2+} toward amyloidogenesis, the toxicity of apo and Ca^{2+}-bound proteins was compared. Under the conditions assayed, native S100A6 was not toxic, regardless of the presence of Ca^{2+} (Fig. 6). However, a significant toxicity is associated with amyloidogenic oligomers obtained at the earlier stages of the growth phase (40% decrease in cell viability). Cellular toxicity decreases upon subsequent fibril maturation: late oligomers still result in a 15% decrease in cell viability but fibrils have no cytotoxic effect. Interestingly, the aggregated species formed in the presence

of Ca^{2+} within all tested growing phases had no effect on cell viability, showing that these aggregates are largely distinct from the amyloidogenic ones formed in its absence.

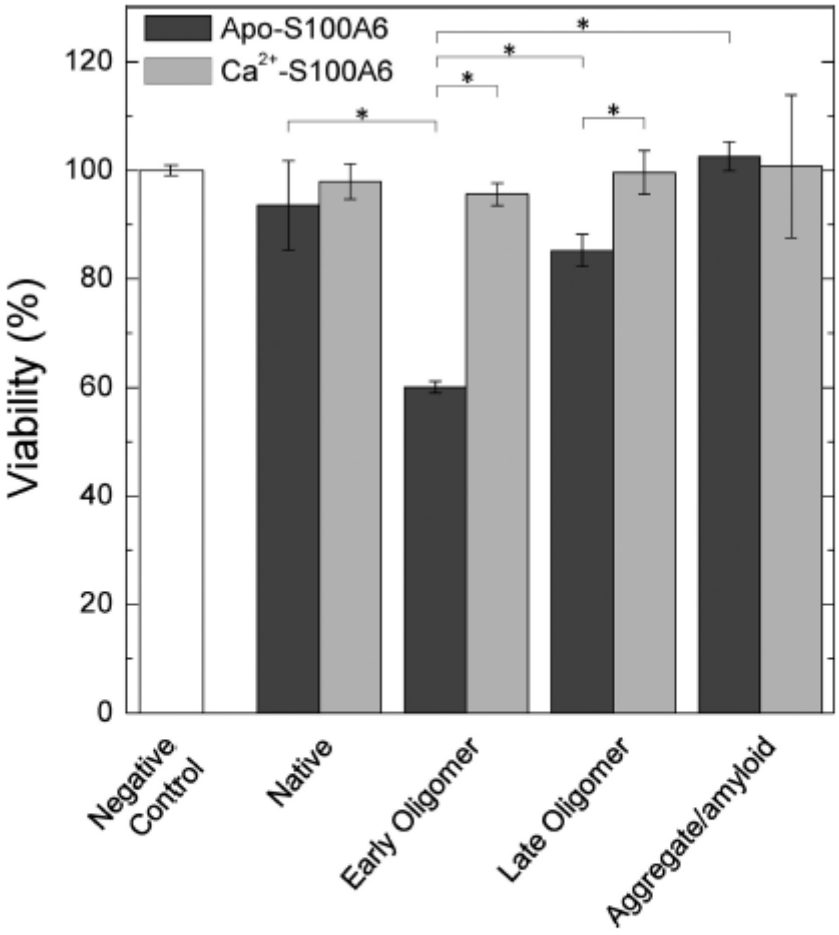

FIGURE 6. **Cytotoxicity of native and amyloid forms of S100A6.** SHSY-5Y neuroblastoma cells were incubated with apo or Ca^{2+}-S100A6 (5 μM) in distinct conformations raised at pH 2.5: native, early oligomer (0.5 h at 57 °C), late oligomer (1 h at 57 °C) or mature aggregate/amyloid (1 week at 57 °C) in the apo or Ca^{2+}-bound states (Fig. 3). Cell viability was assessed after 48 h by the WST-1 reduction assay. Unperturbed cell controls were used to calibrate the measurements. Error bars represent the standard deviation ($n = 3$).*: $p <$ 0.05. Ca^{2+} completely reverts the toxicity of intermediate S100A6 amyloid species.

S100A6 Seeds SOD1 Fibrillization

The formation of S100A6 amyloidogenic oligomers and fibrils might represent a novel mode of S100 mediated central nervous system damage. In fact, the brain of healthy individuals contains protein inclusions called *corpora amylacea*, whose nature is quite unclear, and which contain different S100 proteins, including S100A6 (35). However, protein depositions can also feature pathologic hallmarks in several neurodegenerative human diseases (36). These pathologic aggregates contain a broad mixture of distinct proteins, and are not strictly formed by the protein that is generally associated with the resulting disease. Coincidently, S100A6 is overexpressed in astrocytes closely associated to degenerating motor neurons in ALS patients, where SOD1 enriched cytoplasmic inclusions in are found (11). Although there are no reports of S100A6 being found within these ALS-associated aggregates, the overexpression of S100A6 in ALS models provides a rationale for investigating cross-seeding phenomena between these two proteins.

To test this possibility, we have implemented an aggregation assay based on apo SOD1, the form which is believed to be involved in the onset of ALS pathologic aggregation events. In this assay, carried out at pH 7 and 37 °C, the aggregation kinetics of apo SOD1 was monitored by ThT fluorescence emission. Under these conditions, after a lag phase of 45 h, SOD1 aggregation followed a sigmoidal kinetics with a steady state phase reached after 80 h (Fig. 7). Remarkably, a clear seeding effect occurs when aggregation takes place in the presence of 2% apo S100A6, where the lag phase substantially decreases down to 31 h. S100A6 oligomers have an identical effect. When SOD1 was omitted, no ThT signal variation was measurable. These results suggest that S100A6 can potentiate SOD1 aggregation by favoring the formation of SOD1 amyloid growth nuclei. Eventually, recruitment of astrocytes to the damaged ALS motor neurons resulting in the buildup of S100A6 might trigger interactions between proteins in the complex setting of the synapse (36), especially considering the ability of SOD1 aggregates to propagate in a prion-like manner in neuronal cells (37).

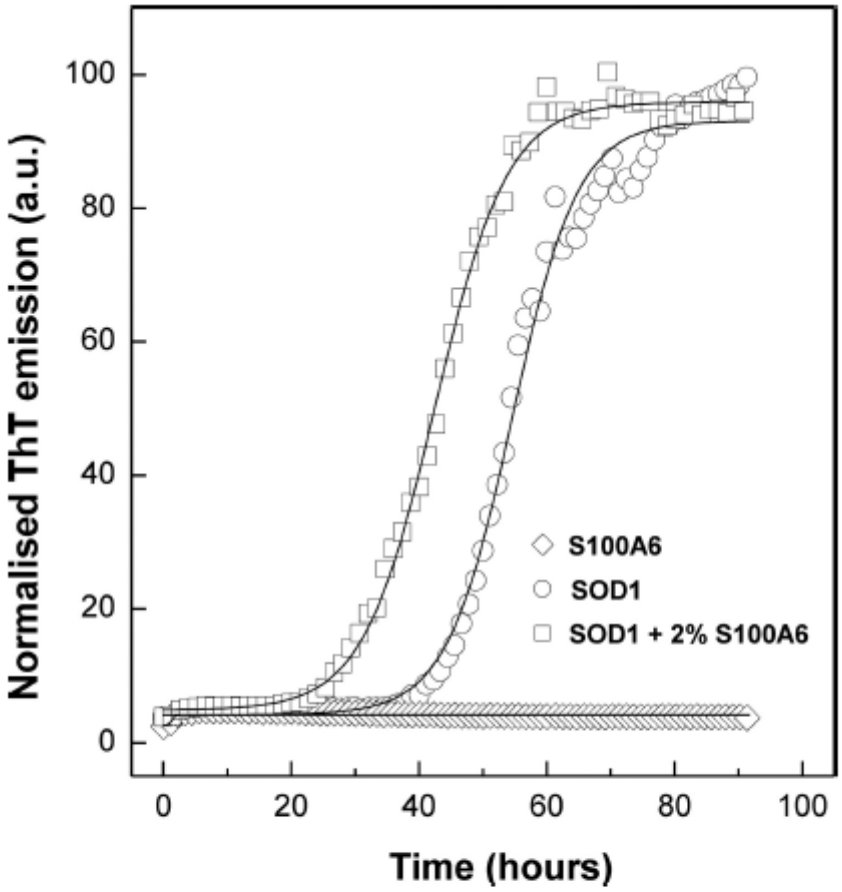

FIGURE 7. **Native S100A6 nucleates SOD1 fibrillization.** The ThT fluorescence assay was used to monitor SOD1 aggregation (50 μM SOD1 at pH 7, 37 °C and under 600 rpm orbital agitation) in the absence (○) and presence of 2% native apo S100A6 (□). Both seeded and un-seeded SOD1 aggregated according to a sigmoidal kinetics with similar slope but the lag phase was shortened in the presence of S100A6 (from 45 h to 31 h). In this assay, S100A6 has a negligible contribution to the ThT fluorescence signal, as judged from the baseline fluorescence signal when SOD1 was omitted (◇).

DISCUSSION

Here we report the ability of the S100A6 cytokine to form amyloid oligomers and fibrils, in a metal ion dependent way, under physiological conditions. S100A6 is a rather stable protein at neutral pH and like other proteins has evolved to minimize its self-aggregation propensity (38, 39). In agreement, computational analysis evidenced a low overall aggregation propensity throughout the S100A6 sequence. Nevertheless, we have collected data showing that transiently populated conformations arising through

native state fluctuations can underpin its conversion into amyloid prone conformers. Indeed, significant aggregation hotspots mapped at helices H_I and H_{IV} within the hydrophobic core. These are involved in inter-subunit contacts for dimer formation and, unlike helices H_{II} andH_{III}, do not undergo substantial conformational changes upon metal binding (40). We thus hypothesize that S100A6 hydrophobic core remodeling yielding amyloid-prone conformers and weaker inter-dimer interactions is an early step in S100A6 fibrillar aggregation. In fact, the importance of dimerization as an amyloidogenic protection mechanism has been highlighted in the S100A8/A9 heterodimer (6), where the overall aggregation propensity of the individual subunits decreases upon heterodimer formation. In agreement, under acidic conditions S100A6 does not unfold but undergoes a series of structural rearrangements, resulting in the buildup of amyloid prone species which directly nucleate aggregation and eliminate a lag phase. At neutral pH, these amyloidogenic intermediate conformations are not readily populated explaining the broadened period of time before nucleation occurs. Also, the absence of a well-defined lag phase suggests a significant aggregation propensity of S100A6 conformers, without the need for destabilizing (*i.e.* non-physiological) conditions to potentiate the aggregation. The aggregation of destabilized (yet native-like) folded globular proteins has been suggested as one of the most relevant mechanisms underlying amyloidogenesis onset, as it does not involve crossing the major energy barrier of unfolding (41). Regarding the cellular effects of these species, the fact is that toxicity induced by native S100 proteins is somehow established in the literature. For example, S100B is known for its concentration-dependent cellular effects in the central nervous system, being neurotrophic at nanomolar levels (42) and inducing apoptosis in a RAGE-dependent manner (43) and exacerbating Aβ neurotoxicity (44) at micromolar concentrations. Following the identification of physiological conditions under which S100A6 forms amyloid fibrils we then moved to inspect the cytotoxicity of these species in particular. We have observed that S100A6 oligomers, and to a lesser extent fibrils, but not native S100A6, affect cell viability. These observations agree with the reported observation that amyloid precursor oligomers are cytotoxic species (45). Specifically, in AD, cognitive impairment is associated with oligomeric Aβ buildup rather than with senile plaque formation. The novelty in our results is the description of increased toxicity associated solely with the amyloid conversion of S100A6. The fact that S100A6 overexpression co-localizes with affected motor neurons in ALS patients (11, 17) prompted us to check its effects on SOD1, another protein involved in this neurodegenerative disease. The observed seeding hints on a putative role of S100A6 in ALS, by propagating pathological SOD1 aggregation. In fact, it is established that S100B oligomers interact with RAGE receptors, which in turn have also the ability to interact with amyloids (46). S100 proteins are actually found in protein inclusions called *corpora amylacea in* brain tissue, but, so far, never in association with disease states. It remains to be shown whether the observations reported here are also true for other S100 proteins. This might open a deeper understanding of the role of S100 proteins in different human disorders.

Indeed, complex interactions between amyloidogenic proteins are likely to play a role in neurodegenerative processes. Interactions between amyloidogenic proteins, similar to the cross-seeding effect herein described for S100A6 and SOD1 have been previously described in the literature, although sometimes with distinct features. In Alzheimer disease, the most characteristic neuropathological hallmarks are the extracellular Aβ plaques and the intracellular neurofibrillary tangles (NFTs), mostly composed by hyperphosphorylated tau protein. Although most cognitive impairment symptoms can be recapitulated by tau aggregation alone, co-aggregation of Aβ in a mouse-model contributes to faster NFT formation, especially in limbic structures, particularly susceptible to NFT-associated lesions (47). Similarly, injection of $A\beta_{1–42}$ fibrils in P301L mutant tau transgenic mice caused a 5-fold increase in NFT number in the cell bodies of neurons projecting into the injection sites (48). Although a physical interaction between Aβ and tau was not unequivocally demonstrated, a direct interaction *in vivo* and *in vitro* between APP and tau, mediated by the Fe65 adaptor protein, was presented (49). Still, N-terminal tau fragments, but not the full-length protein, bind to $Ab_{1–42}$ in the synapse (50). The cellular prion protein (PrP^C) has also been identified as a mediator of Aβ-induced neuronal degeneration *in vivo* by functioning as a cell-surface receptor binding oligomeric Aβ with nanomolar affinity (51). Supporting this hypothesis, insoluble prion protein has been co-purified with forms of $A\beta_{1–42}$ from human Alzheimer disease brain extracts and proposed to be a major Aβ interactor (52). In addition, PrP is expressed in endothelial cells, binds $A\beta_{1–40}$ and mediates transcytosis of the peptide through the blood-brain barrier (53). PrP co-deposits within amyloid core plaques, although neither Aβ or APP co-precipitate with PrP (54). Furthermore, the co-localization of PrP with α-synuclein deposits may indicate that PrP is involved in a general cell stress response toward protein aggregation (55). Along these lines, it has been recently demonstrated that PrP^C

is required for Aβ oligomer-induced neuronal cell death (56). Despite the above mentioned examples, the interaction between amyloidogenic proteins is not always associated with enhanced aggregation. Amyloid cross-seeding between Aβ and amylin (57), a peptide hormone co-secreted with insulin from pancreatic β-cells, may underlie the positive association between Alzheimer disease and diabetes mellitus type II (58), a pathology in which amylin forms amyloid deposits within the pancreas. Nevertheless, non-amyloidogenic amylin conformers are also competent toward $A\beta_{1-40}$ binding and redirect Aβ aggregation toward non-toxic species by shielding Aβ β-sheets from the solvent and driving non-toxic amylin-Aβ co-precipitation (59,–,61). The feasibility of both pro-and anti-aggregation effects is supported by the presence of the soluble forms of both peptides in blood and the cerebrospinal fluid (62), high APP levels in pancreatic extracts (63), presence of hyperphosphorylated tau and aggregated Aβ in Langerhans islets in type 2 diabetes patients (63) as well as co-localization of Aβ and amylin islet amyloid deposits (63).

Extracellular circulating proteins are also involved in amyloidogenic phenomena. Serum amyloid P (SAP) and heparan sulfate proteoglycans (HSPG) co-aggregate in many pathological amyloid deposits (*e.g.* (64,–,67)) and have been implicated in amyloidogenesis. HSPG associate with amyloid precursors, promote misfolding and stabilize nascent fibrils (68, 69). As an example, SAP deposits on the surface of $A\beta_{1-40}$ fibrils, but not protofibrils, *in vitro* but only in the absence of Ca^{2+} (70). In accordance, anti-SAP immunization leads to SAP deposit clearance (71). Also, SAP enhances amyloid A deposition in mice (72) and, together with HSPG, is part of the amyloid fibril core (73, 74). HSPG mediate Aβ binding to the surface of neurons and are involved in its uptake (75), a factor contributing to Aβ cytotoxicity. Altogether, these reports illustrate the extensive regulation of protein aggregation in disease, as well as the importance of non-protein components, as suggested by our results.

The strong effect of Ca^{2+} on the aggregation of S100A6 suggest an important role of this metal ions in the process. Indeed metal ions such as calcium, zinc, and copper are known to play an important role in the process of neurodegeneration also as a result of their interaction with protein oligomers. Briefly, metal ion binding affects protein dynamics, folding and stability and one of their modes of action is by establishing intermolecular interaction critical for the formation of multimeric aggregates. This has been observed to occur in many proteins involved in aggregation disorders and this subject has been extensively addressed in a recent review to which the interested reader can refer to (36). The conformational changes brought about by Ca^{2+} binding to S100A6 provide the structural background to rationalize how its binding modulates amyloid formation. Ca^{2+} binding to S100A6 results in remodeling of surface electrostatics with hydrophobic patch exposure, especially within the aggregation hotspot at helix H_{IV} (40). S100A6 oligomers formed in the presence of Ca^{2+}, which feature anti-parallel β-sheets and decreased α-helix content at the onset of aggregation, are thus off-pathway species in respect to the amyloid fibril forming route. Chelation of Ca^{2+} reverted these structural changes and restored the stability of the S100A6 dimer, shielding the otherwise exposed hydrophobic patches within the core helices. The possibility that hydrophobic core remodeling determines and rate limits S100A6 amyloid fibril formation, may have broader implications within the S100 protein family.

REFERENCES

1. Messerschmidt A., Huber R., Poulos T., Wieghardt K., Fritz G., Heizmann C. W. *(2004) in Handbook of Metalloproteins (Messerschmidt A., Huber R., Poulos T., Wieghardt K. , eds), John Wiley & Sons*
2. Fritz G., Botelho H. M., Morozova-Roche L. A., Gomes C. M. *(2010) Natural and amyloid self-assembly of S100 proteins: structural basis of functional diversity. FEBS J. 277, 4578–4590*
3. Botelho H. M., Koch M., Fritz G., Gomes C. M. *(2009) Metal ions modulate the folding and stability of the tumor suppressor protein S100A2. Febs J. 276, 1776–1786*
4. Santamaria-Kisiel L., Rintala-Dempsey A. C., Shaw G. S. *(2006) Calcium-dependent and -independent interactions of the S100 protein family. Biochem. J. 396, 201–214*
5. Zimmer D. B., Wright Sadosky P., Weber D. J. *(2003) Molecular mechanisms of S100-target protein interactions. Microsc. Res. Tech. 60, 552–559*
6. Yanamandra K., Alexeyev O., Zamotin V., Srivastava V., Shchukarev A., Brorsson A. C., Tartaglia G. G., Vogl T., Kayed R., Wingsle G., Olsson J., Dobson C. M., Bergh A., Elgh F.,

Morozova-Roche L. A. *(2009) Amyloid formation by the pro-inflammatory S100A8/A9 proteins in the ageing prostate. PloS one 4, e5562*

7. Ano Bom A. P., Rangel L. P., Costa D. C., de Oliveira G. A., Sanches D., Braga C. A., Gava L. M., Ramos C. H., Cepeda A. O., Stumbo A. C., De Moura Gallo C. V., Cordeiro Y., Silva J. L. *(2012) Mutant p53 aggregates into prion-like amyloid oligomers and fibrils: implications for cancer. J. Biol. Chem. 287, 28152–28162*
8. Levy C. B., Stumbo A. C., Ano Bom A. P., Portari E. A., Cordeiro Y., Carneiro Y., Silva J. L., De Moura-Gallo C. V. *(2011) Co-localization of mutant p53 and amyloid-like protein aggregates in breast tumors. Int. J. Biochem. Cell Biol. 43, 60–64*
9. Xu J., Reumers J., Couceiro J. R., De Smet F., Gallardo R., Rudyak S., Cornelis A., Rozenski J., Zwolinska A., Marine J. C., Lambrechts D., Suh Y. A., Rousseau F., Schymkowitz J. *(2011) Gain of function of mutant p53 by coaggregation with multiple tumor suppressors. Nat. Chem. Biol. 7, 285–295*
10. Boom A., Pochet R., Authelet M., Pradier L., Borghgraef P., Van Leuven F., Heizmann C. W., Brion J. P. *(2004) Astrocytic calcium/zinc binding protein S100A6 over expression in Alzheimer's disease and in PS1/APP transgenic mice models. Biochim. Biophys. Acta 1742, 161–168*
11. Hoyaux D., Boom A., Van den Bosch L., Belot N., Martin J. J., Heizmann C. W., Kiss R., Pochet R. *(2002) S100A6 overexpression within astrocytes associated with impaired axons from both ALS mouse model and human patients. J. Neuropathol. Exp. Neurol. 61, 736–744*
12. Mori T., Koyama N., Arendash G. W., Horikoshi-Sakuraba Y., Tan J., Town T. *(2010) Overexpression of human S100B exacerbates cerebral amyloidosis and gliosis in the Tg2576 mouse model of Alzheimer's disease. Glia 58, 300–314*
13. Roltsch E., Holcomb L., Young K. A., Marks A., Zimmer D. B. *(2010) PSAPP mice exhibit regionally selective reductions in gliosis and plaque deposition in response to S100B ablation. J. Neuroinflammation 7, 78*
14. Marenholz I., Heizmann C. W., Fritz G. *(2004) S100 proteins in mouse and man: from evolution to function and pathology (including an update of the nomenclature). Biochem. Biophys. Res. Commun. 322, 1111–1122*
15. Leniak W., Słomnicki Ł. P., Filipek A. *(2009) S100A6, new facts and features. Biochem. Biophys. Res. Commun. 390, 1087–1092*
16. Chattopadhyay M., Valentine J. S. *(2009) Aggregation of copper-zinc superoxide dismutase in familial and sporadic ALS. Antioxidants Redox Signaling 11, 1603–1614*
17. Hoyaux D., Alao J., Fuchs J., Kiss R., Keller B., Heizmann C. W., Pochet R., Frermann D. *(2000) S100A6, a calcium- and zinc-binding protein, is overexpressed in SOD1 mutant mice, a model for amyotrophic lateral sclerosis. Biochim. Biophys. Acta 1498, 264–272*
18. Ostendorp T., Leclerc E., Galichet A., Koch M., Demling N., Weigle B., Heizmann C. W., Kroneck P. M., Fritz G. *(2007) Structural and functional insights into RAGE activation by multimeric S100B. EMBO J. 26, 3868–3878*
19. Ahl I. M., Lindberg M. J., Tibell L. A. *(2004) Coexpression of yeast copper chaperone (yCCS) and CuZn-superoxide dismutases in Escherichia coli yields protein with high copper contents. Protein Exp. Purif. 37, 311–319*
20. Potter S. Z., Zhu H., Shaw B. F., Rodriguez J. A., Doucette P. A., Sohn S. H., Durazo A., Faull K. F., Gralla E. B., Nersissian A. M., Valentine J. S. *(2007) Binding of a single zinc ion to one subunit of copper-zinc superoxide dismutase apoprotein substantially influences the structure and stability of the entire homodimeric protein. J. Am. Chem. Soc. 129, 4575–4583*
21. Bradford M. M. *(1976) A rapid and sensitive method for the quantitation of microgram quantities of protein utilizing the principle of protein-dye binding. Anal. Biochem. 72, 248–254*
22. Maurer-Stroh S., Debulpaep M., Kuemmerer N., Lopez de la Paz M., Martins I. C., Reumers J., Morris K. L., Copland A., Serpell L., Serrano L., Schymkowitz J. W., Rousseau F. *(2010) Exploring the sequence determinants of amyloid structure using position-specific scoring matrices. Nat. Methods 7, 237–242*
23. Tartaglia G. G., Vendruscolo M. *(2008) The Zyggregator method for predicting protein aggregation propensities. Chem. Soc. Rev. 37, 1395–1401*
24. Tartaglia G. G., Pawar A. P., Campioni S., Dobson C. M., Chiti F., Vendruscolo M. *(2008) Prediction of aggregation-prone regions in structured proteins. J. Mol. Biol. 380, 425–436*

25. Botelho H. M., Fritz G., Gomes C. M. *(2012) Analysis of S100 oligomers and amyloids. Methods Mol. Biol. 849, 373–386*
26. Morozova-Roche L. A., Zurdo J., Spencer A., Noppe W., Receveur V., Archer D. B., Joniau M., Dobson C. M. *(2000) Amyloid fibril formation and seeding by wild-type human lysozyme and its disease-related mutational variants. J. Struct. Biol. 130, 339–351*
27. Barth A., Zscherp C. *(2002) What vibrations tell us about proteins. Q. Rev. Biophys. 35, 369–430*
28. Berridge M. V., Tan A., S., McCoy K. D., Wang R. *(1996) The biochemical and cellular basis of cell proliferation assays that use tetrazolium salts. Biochemica 4, 14–19*
29. Kayed R., Head E., Sarsoza F., Saing T., Cotman C. W., Necula M., Margol L., Wu J., Breydo L., Thompson J. L., Rasool S., Gurlo T., Butler P., Glabe C. G. *(2007) Fibril specific, conformation dependent antibodies recognize a generic epitope common to amyloid fibrils and fibrillar oligomers that is absent in prefibrillar oligomers. Mol. Neurodegener. 2, 18*
30. Cohen S. I., Vendruscolo M., Dobson C. M., Knowles T. P. *(2012) From macroscopic measurements to microscopic mechanisms of protein aggregation. J. Mol. Biol. 421, 160–171*
31. Goldsbury C., Frey P., Olivieri V., Aebi U., Müller S. A. *(2005) Multiple assembly pathways underlie amyloid-β fibril polymorphisms. J. Mol. Biol. 352, 282–298*
32. Green J. D., Goldsbury C., Kistler J., Cooper G. J., Aebi U. *(2004) Human amylin oligomer growth and fibril elongation define two distinct phases in amyloid formation. J. Biol. Chem. 279, 12206–12212*
33. Cerf E., Sarroukh R., Tamamizu-Kato S., Breydo L., Derclaye S., Dufrêne Y. F., Narayanaswami V., Goormaghtigh E., Ruysschaert J. M., Raussens V. *(2009) Antiparallel β-sheet: a signature structure of the oligomeric amyloid β-peptide. Biochem. J. 421, 415–423*
34. Leclerc E., Fritz G., Weibel M., Heizmann C. W., Galichet A. *(2007) S100B and S100A6 differentially modulate cell survival by interacting with distinct RAGE (receptor for advanced glycation end products) immunoglobulin domains. J. Biol. Chem. 282, 31317–31331*
35. Hoyaux D., Decaestecker C., Heizmann C. W., Vogl T., Schäfer B. W., Salmon I., Kiss R., Pochet R. *(2000) S100 proteins in Corpora amylacea from normal human brain. Brain Res. 867, 280–288*
36. Leal S. S., Botelho H. M., Gomes C. M. *(2012) Metal ions as modulators of protein conformation and misfolding in neurodegeneration. Coordination Chem. Rev. 256, 2253–2270*
37. Münch C., O'Brien J., Bertolotti A. *(2011) Prion-like propagation of mutant superoxide dismutase-1 misfolding in neuronal cells. Proc. Natl. Acad. Sci. U.S.A. 108, 3548–3553*
38. Monsellier E., Chiti F. *(2007) Prevention of amyloid-like aggregation as a driving force of protein evolution. EMBO Rep. 8, 737–742*
39. Rousseau F., Serrano L., Schymkowitz J. W. *(2006) How evolutionary pressure against protein aggregation shaped chaperone specificity. J. Mol. Biol. 355, 1037–1047*
40. Otterbein L. R., Kordowska J., Witte-Hoffmann C., Wang C. L., Dominguez R. *(2002) Crystal structures of S100A6 in the Ca(2+)-free and Ca(2+)-bound states: the calcium sensor mechanism of S100 proteins revealed at atomic resolution. Structure 10, 557–567*
41. Chiti F., Dobson C. M. *(2009) Amyloid formation by globular proteins under native conditions. Nat. Chem. Biol. 5, 15–22*
42. Winningham-Major F., Staecker J. L., Barger S. W., Coats S., Van Eldik L. J. *(1989) Neurite extension and neuronal survival activities of recombinant S100 beta proteins that differ in the content and position of cysteine residues. J. Cell Biol. 109, 3063–3071*
43. Huttunen H. J., Kuja-Panula J., Sorci G., Agneletti A. L., Donato R., Rauvala H. *(2000) Coregulation of neurite outgrowth and cell survival by amphoterin and S100 proteins through receptor for advanced glycation end products (RAGE) activation. J. Biol. Chem. 275, 40096–40105*
44. Kögel D., Peters M., König H. G., Hashemi S. M., Bui N. T., Arolt V., Rothermundt M., Prehn J. H. *(2004) S100B potently activates p65/c-Rel transcriptional complexes in hippocampal neurons: Clinical implications for the role of S100B in excitotoxic brain injury. Neuroscience 127, 913–920*

45. Baglioni S., Casamenti F., Bucciantini M., Luheshi L. M., Taddei N., Chiti F., Dobson C. M., Stefani M. *(2006) Prefibrillar amyloid aggregates could be generic toxins in higher organisms. J. Neurosci. 26, 8160–8167*
46. Fritz G.*(2011) RAGE: a single receptor fits multiple ligands. Trends Biochem. Sci. 36, 625–632*
47. Lewis J., Dickson D. W., Lin W. L., Chisholm L., Corral A., Jones G., Yen S. H., Sahara N., Skipper L., Yager D., Eckman C., Hardy J., Hutton M., McGowan E. *(2001) Enhanced neurofibrillary degeneration in transgenic mice expressing mutant tau and APP. Science 293, 1487–1491*
48. Götz J., Chen F., van Dorpe J., Nitsch R. M. *(2001) Formation of neurofibrillary tangles in P301l tau transgenic mice induced by Aβ 42 fibrils. Science 293, 1491–1495*
49. Barbato C., Canu N., Zambrano N., Serafino A., Minopoli G., Ciotti M. T., Amadoro G., Russo T., Calissano P. *(2005) Interaction of tau with Fe65 links tau to APP. Neurobiology Disease 18, 399–408*
50. Amadoro G., Corsetti V., Atlante A., Florenzano F., Capsoni S., Bussani R., Mercanti D., Calissano P. *(2012) Interaction between NH(2)-tau fragment and Aβ in Alzheimer's disease mitochondria contributes to the synaptic deterioration. Neurobiology Aging 33, 833*
51. Laurén J., Gimbel D. A., Nygaard H. B., Gilbert J. W., Strittmatter S. M. *(2009) Cellular prion protein mediates impairment of synaptic plasticity by amyloid-β oligomers. Nature 457, 1128–1132*
52. Zou W. Q., Xiao X., Yuan J., Puoti G., Fujioka H., Wang X., Richardson S., Zhou X., Zou R., Li S., Zhu X., McGeer P. L., McGeehan J., Kneale G., Rincon-Limas D. E., Fernandez-Funez P., Lee H. G., Smith M. A., Petersen R. B., Guo J. P. *(2011) Amyloid-β42 interacts mainly with insoluble prion protein in the Alzheimer brain. J. Biol. Chem. 286, 15095–15105*
53. Pflanzner T., Petsch B., André-Dohmen B., Müller-Schiffmann A., Tschickardt S., Weggen S., Stitz L., Korth C., Pietrzik C. U. *(2012) Cellular prion protein participates in amyloid-β transcytosis across the blood-brain barrier. J. Cerebral Blood Flow Metabolism 32, 628–632*
54. Ferrer I., Blanco R., Carmona M., Puig B., Ribera R., Rey M. J., Ribalta T. *(2001) Prion protein expression in senile plaques in Alzheimer's disease. Acta Neuropathology 101, 49–56*
55. Kovacs G. G., Zerbi P., Voigtländer T., Strohschneider M., Trabattoni G., Hainfellner J. A., Budka H. *(2002) The prion protein in human neurodegenerative disorders. Neurosci. Letts. 329, 269–272*
56. Kudo W., Lee H. P., Zou W. Q., Wang X., Perry G., Zhu X., Smith M. A., Petersen R. B., Lee H. G. *(2012) Cellular prion protein is essential for oligomeric amyloid-β-induced neuronal cell death. Hum. Mol. Genet. 21, 1138–1144*
57. O'Nuallain B., Williams A. D., Westermark P., Wetzel R. *(2004) Seeding specificity in amyloid growth induced by heterologous fibrils. J. Biol. Chem. 279, 17490–17499*
58. Nicolls M. R. *(2004) The clinical and biological relationship between Type II diabetes mellitus and Alzheimer's disease. Curr. Alzheimer Res. 1, 47–54*
59. Rezaei-Ghaleh N., Andreetto E., Yan L. M., Kapurniotu A., Zweckstetter M. *(2011) Interaction between amyloid β peptide and an aggregation blocker peptide mimicking islet amyloid polypeptide. PLoS One 6, e20289*
60. Yan L. M., Velkova A., Tatarek-Nossol M., Andreetto E., Kapurniotu A. *(2007) IAPP mimic blocks Abeta cytotoxic self-assembly: cross-suppression of amyloid toxicity of Aβ and IAPP suggests a molecular link between Alzheimer's disease and type II diabetes. Angew Chem. Int. Ed. Engl. 46, 1246–1252*
61. Seeliger J., Evers F., Jeworrek C., Kapoor S., Weise K., Andreetto E., Tolan M., Kapurniotu A., Winter R. *(2012) Cross-amyloid interaction of Aβ and IAPP at lipid membranes. Angew Chem. Int. Ed. Engl. 51, 679–683*
62. Andreetto E., Yan L. M., Caporale A., Kapurniotu A. *(2011) Dissecting the role of single regions of an IAPP mimic and IAPP in inhibition of Aβ40 amyloid formation and cytotoxicity. Chembiochem. 12, 1313–1322*
63. Miklossy J., Qing H., Radenovic A., Kis A., Vileno B., Laszlo F., Miller L., Martins R. N., Waeber G., Mooser V., Bosman F., Khalili K., Darbinian N., McGeer P. L. *(2010) Beta amyloid and hyperphosphorylated tau deposits in the pancreas in type 2 diabetes. Neurobiol. Aging 31, 1503–1515*

64. Shi J., Perry G., Berridge M. S., Aliev G., Siedlak S. L., Smith M. A., LaManna J. C., Friedland R. P. *(2002) Labeling of cerebral amyloid β deposits in vivo using intranasal basic fibroblast growth factor and serum amyloid P component in mice. J. Nuclear Med. 43, 1044–1051*
65. Moss J., Shore I., Woodrow D. *(1994) AA glomerular amyloid. An ultrastructural immunogold study of the colocalization of heparan sulphate proteoglycan and P component with amyloid fibrils together with changes in distribution of type IV collagen and fibronectin. Histopathology 24, 427–435*
66. Pepys M. B., Booth D. R., Hutchinson W. L., Gallimore J. R., Collins I. M., Hohenester E. *(1997) Amyloid P component. A critical review. Amyloid 4, 274–295*
67. Zhang X., Li J. P.*(2010) Heparan sulfate proteoglycans in amyloidosis. Progr. Mol. Biol. Translat. Sci. 93, 309–334*
68. Ancsin J. B.*(2003) Amyloidogenesis: historical and modern observations point to heparan sulfate proteoglycans as a major culprit. Amyloid 10, 67–79*
69. Inoue S., Kawano H., Ishihara T., Maeda S., Ohno S. *(2005) Formation of experimental murine AA amyloid fibrils in SAP-deficient mice: high resolution ultrastructural study. Amyloid 12, 157–163*
70. Holm Nielsen E., Nybo M., Junker K., Toftedal Hansen P., Rasmussen I. M., Svehag S. E. *(2000) Localization of human serum amyloid P component and heparan sulfate proteoglycan in in vitro-formed Aβ fibrils. Scand. J. Immunol. 52, 110–112*
71. Bodin K., Ellmerich S., Kahan M. C., Tennent G. A., Loesch A., Gilbertson J. A., Hutchinson W. L., Mangione P. P., Gallimore J. R., Millar D. J., Minogue S., Dhillon A. P., Taylor G. W., Bradwell A. R., Petrie A., Gillmore J. D., Bellotti V., Botto M., Hawkins P. N., Pepys M. B. *(2010) Antibodies to human serum amyloid P component eliminate visceral amyloid deposits. Nature 468, 93–97*
72. Togashi S., Lim S. K., Kawano H., Ito S., Ishihara T., Okada Y., Nakano S., Kinoshita T., Horie K., Episkopou V., Gottesman M. E., Costantini F., Shimada K., Maeda S. *(1997) Serum amyloid P component enhances induction of murine amyloidosis. Lab. Investig. 77, 525–531*
73. Inoue S., Kisilevsky R. *(1996) A high resolution ultrastructural study of experimental murine AA amyloid. Lab. Investig. 74, 670–683*
74. Inoue S., Kuroiwa M., Tan R., Kisilevsky R. *(1998) A high resolution ultrastructural comparison of isolated and in situ murine AA amyloid fibrils. Amyloid 5, 99–110*
75. Kanekiyo T., Zhang J., Liu Q., Liu C. C., Zhang L., Bu G. *(2011) Heparan sulphate proteoglycan and the low-density lipoprotein receptor-related protein 1 constitute major pathways for neuronal amyloid-β uptake. J. Neurosci. 31, 1644–1651*